Aalborg Universitet

AALBORG UNIVERSITY
DENMARK

Revealing the atomistic origin of the disorder-enhanced Na-storage performance in NaFePO4 battery cathode

Xiong, F.Y.; An, Q.Y.; Xia, L.X.; Zhao, Y.; Mai, L.Q.; Tao, H.Z.; Yue, Yuanzheng

Author's Accepted Manuscript

Revealing the atomistic origin of the disorder-enhanced Na-storage performance in NaFePO$_4$ battery cathode

Fangyu Xiong, Qinyou An, Lixue Xia, Yan Zhao, Liqiang Mai, Haizheng Tao, Yuanzheng Yue
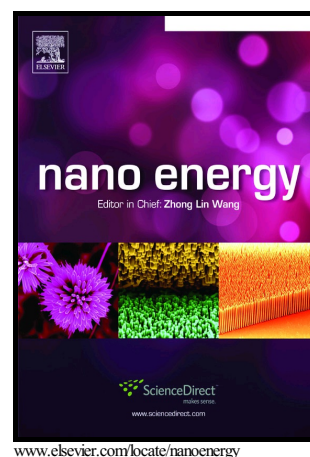
Cite this article as: Fangyu Xiong, Qinyou An, Lixue Xia, Yan Zhao, Liqiang Mai, Haizheng Tao and Yuanzheng Yue, Revealing the atomistic origin of the disorder-enhanced Na-storage performance in NaFePO$_4$ battery cathode, *Nano Energy*, https://doi.org/10.1016/j.nanoen.2018.12.087

This is a PDF file of an unedited manuscript that has been accepted for publication. As a service to our customers we are providing this early version of the manuscript. The manuscript will undergo copyediting, typesetting, and review of the resulting galley proof before it is published in its final citable form. Please note that during the production process errors may be discovered which could affect the content, and all legal disclaimers that apply to the journal pertain.

Revealing the atomistic origin of the disorder-enhanced Na-storage performance in NaFePO$_4$ battery cathode

Fangyu Xiong[1,2], Qinyou An[2], Lixue Xia[1,3], Yan Zhao[1,3], Liqiang Mai[2,3], Haizheng Tao[1,*],

Yuanzheng Yue[1,4,*]

[1]State Key Laboratory of Silicate Materials for Architectures, Wuhan University of Technology, Wuhan 430070, China

[2]State Key Laboratory of Advanced Technology for Materials Synthesis and Processing, Wuhan University of Technology, Wuhan 430070, China

[3]International School of Materials Science and Engineering, Wuhan University of Technology, Wuhan 430070, China

[4]Department of Chemistry and Bioscience, Aalborg University, DK-9220 Aalborg, Denmark

thz@whut.edu.cn (Prof. H.Z. Tao);

yy@bio.aau.dk (Prof. Y.Z. Yue)

 *Corresponding Authors:

Abstract:

Among the various SIBs cathode materials, NaFePO$_4$ attracts much attention owing to its high theoretical capacity (155 mAh g^{-1}), low cost, high structural stability, and non-toxicity. Nevertheless, the NaFePO$_4$ with maricite structure, thermodynamically stable phase, has been considered as electrochemically inactive for sodium-ion storage. In this work, we succeeded in tuning the degree of disorder in NaFePO$_4$ cathode material by a mechanochemical route to enhance electrochemical performances of Na-ion batteries. The derived NaFePO$_4$ cathodes containing both amorphous and maricite phases exhibit much improved sodium storage performance with an initial capacity of 115 mAh g^{-1} at 1 C and an excellent cycling stability of capacity retention of 91.3% after 800 cycles. By X-ray absorption near edge and Raman spectroscopy, we revealed the atom-scale structural origin of the enhanced Na-storage performances of the amorphous NaFePO$_4$ electrode. The transformation of edge-sharing FeO$_6$ octahedra into various FeO$_n$ polyhedra upon amorphization was found to be a key to attain the superior performances for Na ion batteries.

Graphical abstract
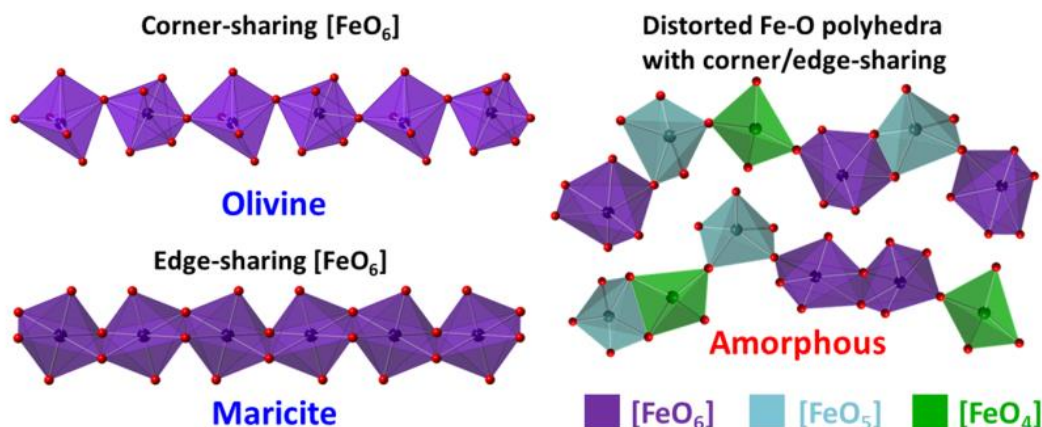
Introduction

Owing to their potential broad applications in power tools, electric vehicles, and solar energy setup, $LiFePO_4$ compounds have attracted much attention of energy scientists and technologists. The major commercial advantages of these compounds originate from their thermodynamically stable olivine structure. This structure exhibits high stability against charging/discharging cycling, and even at high temperatures, gives the safety of batteries in repeated high-current discharge rate applications, and can be economically generated [1-4]. Driven by the large-scale energy storage ability and the abundant cheap resources of sodium, Na ion batteries have been considered as a promising alternative to Li ion batteries [5-11]. According to literatures [12-14], it was possible to fabricate the olivine $NaFePO_4$ as high-performance cathode with high theoretical capacity (155 mAh g^{-1}) for Na ion batteries, however, the complexity of the fabrication process impeded its application. The thermodynamically stable olivine phase in the Li bearing iron phosphate compounds, which contain one-dimensional channels for Li diffusion, is not favored in the sodium analogue [14, 15]. The thermodynamically favorable phase in the Na counterpart is the maricite, which has been experimentally found to be electrochemically inactive under normal battery operating voltages (0~4.5 V). Its electrochemical inactivity has been attributed to the fact that the cavities with trapped Na ions are not connected by pathways [16].

However, it was remarkable that maricite $NaFePO_4$ could be transformed into amorphous phase through the first charging at 4.5 V holding for 5 hrs [17]. By this transformation, the battery with $NaFePO_4$ cathode reached a reversible capacity of 142 mAh g^{-1} (92% of the theoretical value) at 0.05 C at the first cycle and an outstanding cyclability with a 95% retention after 200 cycles. This unexpected performance was ascribed to the highly electrochemical active amorphous $NaFePO_4$ phase, in which the hopping active barrier of Na^+ is about 20% of that of the maricite $NaFePO_4$ phase according to the quantum mechanics calculations. This discovery intrigues much interest of scientists in amorphization of maricite $NaFePO_4$ by many routes. Recently, using a similar amorphization method, Liu *et al*. further enhanced the desodiation by minimizing the size of the precursor maricite $NaFePO_4$ through the electro-spinning technique [18]. They achieved the capacity of 145 mAh g^{-1} at 0.2 C, the rate capability of 61 mAh g^{-1} at 50 C, and unprecedentedly high cycling stability, i.e., 89% capacity retention after 6300 cycles. Honma *et al*.[19] found that the cathode performances of sodium iron phosphate glass can be enhanced by increasing the FeO content and thereby attained a maximum capacity of 115 mAh g^{-1} at 0.1 C for the $40FeO \cdot 60NaPO_3$ glass. However, the $NaFePO_4$ glass has not been successfully made by the conventional melt-quenching technique due to the strong tendency of its melt to crystallize. It was found that mechanochemical treatment, i.e., planetary ball milling could activate, i.e., introduce disorder into $NaFePO_4$ and thereby enhanced its electrochemical properties [20, 21].

It is worth mentioning that the disorder/order engineering concept was recently introduced by Zhang et al to enhance the electrochemical performances of glassy anodes for lithium ion battery [22]. In contrast to inducing the disorder in crystalline $NaFePO_4$ via battery high potential charging [17, 18], ball-milling [20, 21] and melt-quenching [19], they found that a certain degree of order (nano-crystals) in the glass phase can be induced by the first few cycles of charging/discharging, and the cyclability of the anode was improved.

Despite numerous studies, the structural origin of amorphous $NaFePO_4$ as a high-active cathode for Na-ion batteries remains unrevealed. In this work, we fabricate the polymorphic $NaFePO_4$ composites (containing maricite, amorphous phase and carbon) by the mechanochemical method as the cathode materials of Na-ion batteries. The composites with different degrees of

disorder were synthesized and used to clarify the relation between amorphous phase and sodium storage capacity. The polymorphic composite with optimized milling parameters displays an enhanced sodium storage capacity of 115 mAh g^{-1} and excellent cycling stability reflected by the capacity retention of 91.3% after 800 cycles. To discover the atomistic origin of disordered $NaFePO_4$ with enhanced cathode performances, we performed structural characterizations on the three $NaFePO_4$ phases including maricite, olivine, and amorphous phase by X-ray absorption near edge (XANE) and Raman spectroscopy. Base on the characterization results, we propose a structural model of purely amorphous $NaFePO_4$ to explain the activated sodium storage capacity.

Experimental Section

Samples synthesis

Maricite $NaFePO_4$ was synthesized according to the following procedure. $FeSO_4 \cdot 7H_2O$, $NaH_2PO_4 \cdot 2H_2O$ and citric acid (all are analytically pure and purchased from Sinopharm Chemical Reagent Co., Ltd. Shanghai, China) with the 1:1:1.5 molar ratio were dissolved into deionized water. After stirring vigorously for 10 min, the solution was heated to 160 °C and hold for 12 hrs to obtain the dried precursor. Then the precursor was heat-treated at 300 °C in air for 4 hrs and further calcined at 600 °C in Ar for 10 hrs. Finally, the polymorphic composites were obtained using a high-energy planetary ball mill (Pulverisette-7 premium line; Fritsch, Idar-Obserstein, Germany) at 800 rpm for 5, 10, 15, 20, 25 hrs. The mass ratio of the powder and ZrO_2 balls (3 mm in diameter) is ~1:15. To avoid agglomeration, 1.5 mL isopropyl alcohol was added to the pot as an inert process control agent, which had little influence on the milled sample structure [23, 24].

Olivine $NaFePO_4$ was obtained from olivine $LiFePO_4$ via chemical delithiation and followed by sodiation [13, 14]. The $LiFePO_4$ was synthesized by the same procedure of maricite $NaFePO_4$ with replacing $NaH_2PO_4 \cdot 2H_2O$ by LiH_2PO_4 (99%, Aladdin). The chemical delithiation and sodiation processes were performed in a glove box. The 0.1 g synthesized $LiFePO_4$ was added into a solution of 0.2 g NO_2BF_4 (98%, Sigma-Aldrich) in 10 mL acetonitrile (99.8%, Sinopharm). After stirring for 24 hrs, the delithiated $LiFePO_4$ powder was obtained via filtering and drying. Then, the delithiated $LiFePO_4$ was added into a solution of 0.3 g NaI (99.0%, Sinopharm) in 10 mL

acetonitrile, and the mixture was stirred at 60 ℃ for 48 hrs. Finally, the olivine $NaFePO_4$ was obtained after filtered and dried.

Materials characterization

X-ray diffraction (XRD) measurements were performed to investigate the crystallographic structure using a D8 Advance X-ray diffractometer with a nonmonochromated Cu Kα X-ray source. Field emission scanning electron microscopy (FESEM) images were collected with a JEOL-7100F microscope at an acceleration voltage of 20 kV. Transmission electron microscopy (TEM), high resolution TEM (HRTEM), high-angle annular dark field scanning transmission electron microscopy (HAADF-STEM) images and Energy dispersive spectrometer (EDS) mapping were recorded by using a Titan G2 60-300 microscope. Raman spectra were obtained using a HORIBA LabRAM HR Evolution micro-Raman spectroscopy system with the 633 nm laser. The carbon content analyses were performed by Elementar Vario EL cube elemental analyzer. The differential scanning calorimetry (DSC) analysis was performed at 10 K min^{-1} to a certain temperature in Ar using STA 449 F1 thermal analyzer. The Na K- and O K-edge X-ray absorption near edge structure spectra (XANES) were measured in fluorescence mode at beamline 4B7B (soft X-ray) of Beijing Synchrotron Radiation Facility (BSRF).

Computational method

All calculation on $NaFePO_4$ were conducted by Generalized Gradient Approximation (GGA) with the Perdew–Burke–Ernzerhof (PBE) [25] exchange-correlation parameterization to Density Functional Theory (DFT) using $Dmol^3$ code [26]. The 5.0 Å global Orbital cutoff was employed as the maximum value from all the cutoffs specific to each element in this system, and meanwhile a (1 × 1 × 1) k-point grid was applied. DFT Semi-core Pseudopots (DSPPs) were used to describe the interactions between valence electrons and ionic cores. The geometry optimization parameters for the total energy convergence and the max ionic force were 10^{-5} Ha and 2×10^{-5} Ha $Å^{-1}$, respectively. The nudged elastic band (NEB) [27] method was employed to obtain the minimum energy paths (MEPs) of Na jumps between the corresponding neighboring sites. A threshold of 0.02 Ha $Å^{-1}$ was set for the total force acting on the NEB images of the interpolated reaction paths.

Battery assembling and electrochemical characterization

CR2016-type coin cells were assembled in a glove box ($O_2 \leq 1$ ppm and $H_2O \leq 1$ ppm), which used the sodium foil as the anode and the glassy fiber (GF/D Whatman) as the separator. The electrolyte was composed of 1 M $NaPF_6$ dissolved in EC (ethylene carbonate)/PC (propylene carbonate) with volume ratio of 1:1. Cathodes were obtained with 60% as-synthesized active materials, 30% acetylene black and 10% poly(tetrafluoroethylene) (PTFE), and the mass loading of active material was about 3–4 mg cm^{-2}. Electrochemical performances were characterized by measuring the galvanostatic charge/discharge cycling behavior in a potential range of 1.5–4.5 V (vs. Na^+/Na) with a multichannel battery testing system (LAND CT2001A). The cyclic voltammetry (CV) curves were obtained by using a VMP3 multichannel electrochemical workstation (Bio-Logic France).

Results

Electrochemical performances

The coin-type cells with sodium metal anode were assembled to evaluate the sodium storage performance of the as-prepared maricite $NaFePO_4$ and the milling-derived polymorphic composites with different degrees of disorder obtained at 800 rpm for 5, 10, 15, 20 and 25 hrs. Galvanostatic discharge/charge cycles and corresponding charge/discharge curves of the six samples at 1 C (1 C = 155 mA g^{-1}) in the potential range of 1.5-4.5 V are shown in Fig. 1a and Fig. S1, respectively. Similar to previous studies [16], the as-prepared maricite $NaFePO_4$ delivered a maximum specific capacity of 36 mAh g^{-1} for the initial discharge and rapidly drop to 18 mAh g^{-1} for the second discharge, meaning that the maricite $NaFePO_4$ is electrochemically inactive, due to the absence of channels for sodium transport in the closed maricite framework [14]. Through the high-energy ball-milling approach, the obtained polymorphic composites exhibit enhanced specific capacities, i.e., 50 mAh g^{-1} by milling for 5 hrs, 75 mAh g^{-1} for 10 hrs, up to about 115 mAh g^{-1} for 15, 20 or 25 hrs. Hereafter, we focused on the characteristics of the polymorphic composites obtained by milling for 15 hrs (NFP-15). As indicated by the charge/discharge curves at 1 C (Fig. 1b), NFP-15 displays a slope plateau with an average potential of about 2.5 V, which is in line with the previously reported results [17].The broad redox peaks can be seen in the CV curves of NFP-15 (Fig. S2), and correspond to the slope plateaus. Even after 800 cycles at 1 C, NFP-15 still delivers a high reversible capacity of 105 mAh g^{-1} (Fig. 1c), and the capacity retention of 91.3%. This cycling

life is longer than that of the most reported maricite NaFePO$_4$ based materials [16, 17, 19, 21, 28]. Besides, this cycling performance is better than that of many reported crystal Fe-based cathode materials for sodium-ion battery (Table S1), indicating the superiority of as-synthesized polymorphic NaFePO$_4$ composites [29-34]. In Fig. 1d, we can see the feasibility of the NFP-15 composite for high power applications, since it exhibits the capacity of 52 mAh g^{-1} even at the rate of 10 C, which can quickly return to a higher level of 67, 90 and 100 mAh g^{-1} at 5 C, 2 C and 1 C, respectively.

Structure of polymorphic composites

XRD analysis (Fig. S3) of as-prepared maricite sample gives the evidence for the pure single phase, i.e., the maricite-type NaFePO$_4$ phase (JCPDS No. 029-1216). The HRTEM image of this as-prepared sample (Fig. 2e) further verifies the existence of the single phase as we can see a clear lattice fringe with inter-planar distance of 2.69 Å corresponding to the d-space of (211) facets of maricite-type NaFePO$_4$. Furthermore, the HRTEM image of the as-synthesized samples (Fig. S4a) indicates a non-uniform size distribution of NaFePO$_4$ nanoparticles in the range from 100 to 600 nm embedded in the carbon matrix. Finally, according to the CHN elemental analysis, the carbon content of as-synthesized samples is around 10 wt%. Considering the theoretical densities of carbon and maricite NaFePO$_4$ (about 1.80-2.00 [35] and 3.69 [36, 37] g cm^{-3}, respectively), the volume fraction of carbon should be higher than 20% (percolation threshold), implying that the percolation networks of carbon is established.

Through a high-energy ball-milling approach, we can partially amorphize the as-synthesized maricite-type NaFePO$_4$. As shown in Fig. S1, after milling at 800 rpm for 5, 10, 15, 20 and 25 hrs, all the XRD patterns show a similar profile, i.e., the sharp diffraction peaks disappear except for the weak and broad peak located at about 33°, indicating the partial amorphization. HRTEM images of these samples (Fig. 2f, g; Fig. S4f) further demonstrate the structural characteristics of polymorphic composites. Atomic-scale indiscernible interfaces imply that there is the chemical bonding between the embedded maricite and amorphous matrix NaFePO$_4$. The stronger mixed ionic and covalent bonds of P-O or Fe-O in the interfacial region should play a key role in enhancing the

electrochemical cycling stability. This maricite/amorphous composite structure may improve the crack resistance by blocking the propagation of localized shear bands, and then enhance cycling stability by alleviating the crack-induced capacity fading [38-40]. After 100 cycles at 1 C, the ordered nano-domains can also be observed in the HRTEM image for NFP-15 (Fig. S5), indicating the good stability of maricite/amorphous composite structure. By controlling the ball-milling durations, we were able to modulate the interfacial density and the degree of disorder for NaFePO$_4$. According to FESEM images (Fig. 2a-c, Fig. S6), the morphological evolution with an increase of milling duration can be viewed from the irregular particles with several micrometers to sub-micrometer particles. By further increasing the duration after milling for 15 hrs, we did not achieve a distinct reduction in particle size, but observed a slight self-agglomeration. This means that it gets more difficult to reduce the particle size further just by increasing ball-milling time. Such a morphological evolution can be further verified by the TEM images (Fig. 2d; Figs. S4 a-e).

EDS mapping (Fig. 2h) demonstrates a uniform Na, Fe, P, O, and C element distribution in the polymorphic composite. The existence of the carbon phase can be further verified by the two characteristic bands (bands D and G) in the range of 1200-1700 cm^{-1} on the Raman spectra (Fig. S7a) [41, 42]. The ratio of intensity for D and G bands can be used as an indicator of the structural evolution. However, there is no distinguishable spectral difference among the samples milled for various durations, i.e., milling did not cause a detectable structural change. Moreover, the spectrum of NFP-15 has been deconvoluted into three peaks by fitting, and the ~1500 cm^{-1} peak was assigned to amorphous sp^2-bonded forms of carbon (Fig. S7b) [43].

Transitions between NaFePO$_4$ polymorphs

For the as-synthesized maricite-type NaFePO$_4$, which is the thermodynamically stable phase, no detectable calorimetric response occur during heating to 600 ℃ (Fig. 3a). In contrast, for the metastable olivine-type phase of NaFePO$_4$ (exhibited by the XRD pattern in Fig. S8), which cannot be prepared by the conventional synthetic routes [17, 44], an exothermic peak occurs between 470 and 520 ℃ during the first DSC upscan. This result implies that the metastable olivine-type phase is transformed into the stable maricite-type NaFePO$_4$ [45]. However, the transition is

thermodynamically irreversible, and this is confirmed by the second up-scanning (Fig. 3a). For the polymorphic composite NFP-15, an even larger exothermic peak appears between 365 to 465 ℃, reflecting the higher potential energy state of the amorphous $NaFePO_4$ phase [46] compared to the olivine-type phase. In addition, prior to the sharp exothermic response (i.e., crystallization), we did not observe the glass transition. The sharp exotherm suggests that the amorphous $NaFePO_4$ is extremely unstable against crystallization, i.e., $NaFePO_4$ is a poor glass former, and this was also confirmed by the inability to vitrify $NaFePO_4$ by melt-quenching [19].

With extending the milling duration, the exotherm is enhanced (Fig. 3b), implying that the degree of disorder increases in $NaFePO_4$. Furthermore, the exotherm enhancement could originate from the milling-induced rupture and distortion of chemical bonds. To further identify the atomic-scale structural change of the polymorphic composites compared to the maricite and olivine $NaFePO_4$, we acquired XANE spectra for Na K-edge and O K-edge and the Raman spectra, as shown in Fig. 4.

Discussions

Structural order to disorder transition in $NaFePO_4$ phases

The Na K-edge XANE spectra of $NaFePO_4$ polymorphic composites obtained by milling at 800 rpm for 5, 10, 15, 20, and 25 hrs are similar to that of the maricite phase (Fig. 4a, Fig. S9), but clearly differ from that of olivine $NaFePO_4$. This result suggests that the nearest coordination environment of Na in the milling-induced amorphous $NaFePO_4$ phase is similar to that in the as-prepared maricite phase.

Regarding the O component (Fig. 4b), the O K-edge XANE spectrum for NFP-15 is more similar to that of maricite $NaFePO_4$ compared to olivine $NaFePO_4$. This means that the nearest coordination number of O with Na, Fe and P in amorphous $NaFePO_4$ phase is closer to that of maricite $NaFePO_4$. According to the dipole selection rule, the O K-edge XANE spectra are due to transitions from atomic-like 1s state to unoccupied bound and free states with p-character [47, 48]. The sharp peak at about 534 eV should be mainly related to the transition metal Fe 3d states [47, 48]. The intensity of this peak increases in the order of olivine, maricite and NFP-15 (Fig. 4b).

Considering the drop of coordination number of O from olivine type (completely 4) to maricite type (4 and 3) $NaFePO_4$, the highest intensity of this peak for the NFP-15 should be due to the further decrease of the nearest coordination number of O compared to the maricite type phase. This change might be mainly due to the enhancement of hybridization of Fe 3d states and O 2p states [47], following the decrease of the coordination number of partial Fe after amorphization. This inference can be confirmed by the Raman spectra (analyzed below), where the shortening of Fe-O bond length following the reduction of the coordination number is a reflection of the enhancement of hybridization of Fe 3d states and O 2p states.

The similarity of the positions and patterns of characteristic Raman peaks, located at about 950, 1000, 450, and 600 cm^{-1}, which are attributed to the four vibrational modes of isolated PO_4^{3-} units, indicates that isolated PO_4^{3-} structural units remain unaffected during milling-induced amorphization process [19, 49, 50]. This preservation of local coordination surroundings in P should arise from the stable and strong P-O covalent bonds.

As shown in Fig.4c, we can see an obvious evolution of the characteristic peaks in the region 200 ~ 400 cm^{-1}. In contrast to the two weak peaks in this region for the olivine-type $NaFePO_4$, three strong peaks at 217, 275 and 390 cm^{-1} appears for the maricite-type one. This differences should be ascribed to the different FeO_6 connecting patterns: corner sharing in olivine-type phase and bridge sharing in maricite-type phase [50-52]. Upon only 5 hrs milling (Fig.S10), the characteristic peak at 390 cm^{-1} disappears. In addition, following the increase of milling time, the other two peaks at 217 and 275 cm^{-1} become weaker and wider. These evolution indicates that the nearest coordinative surroundings of Fe are easy to be changed. Possibly due to relatively weaker Fe-O bonds compared to the P-O ones, the ordered FeO_6 edge-sharing octahedral chains in the maricite-type phase can be easily altered upon milling. And except for the distorted FeO_6 octahedra, milling may induce other types of Fe-O polyhedra, e.g., tetrahedra and pentahedra.

Therefore, through the milling-induced amorphization, the short-range order of the amorphous $NaFePO_4$ is similar to that of the maricite-type one, except the distinct evolution of coordination number of Fe from 6 in maricite type to mainly 4, 5 and 6 in the amorphous one [51].

Mechanism of unlocked sodium storage for amorphous NaFePO₄ phase

Originating from its one-dimensional diffusion tunnel for Na ions (Fig. 5b), metastable olivine NaFePO$_4$ can offer a high theoretical capacity of 155 mAh g^{-1} and an operating potential of 2.9 V (vs Na$^+$/Na) based on the single electron reaction of the Fe$^{3+/2+}$ couple. However, due to the blocked ionic diffusion channels between ordered Na sites (Fig. 5c) with high diffusive activation barrier, the deintercalation/intercalation of Na ions in thermodynamically stable maricite NaFePO$_4$ are not favorable under the normal battery operating conditions, and hence this NaFePO$_4$ phase is electrochemical inactive. Upon milling, the derived amorphous NaFePO$_4$ exhibits better electrochemical activity due to the enhancement of Na mobility. Different from the mechanism of Na ionic transportation in olivine phase, the higher Na diffusivity in amorphous NaFePO$_4$ compared to the ordered maricite one should be associated with the statistical distortion and asymmetry of Na surroundings (Fig. 5a). Based on the above-mentioned structural analysis of amorphous NaFePO$_4$, the statistical distortion and asymmetry of Na sites could result from the broader distribution of Fe- or P-O bonds, and especially the alterations of coordination number of Fe from 6 in maricite type to mainly 4, 5 or 6 co-existing in amorphous type. It is the statistical distortion and asymmetry of Na sites that lead to the enhancement of potential energy and instability of Na sites, and hence, to reduction of activation barrier for Na hopping, resulting in a realization of reversible insertion/extraction of Na$^+$ under normal battery operating conditions.

Moreover, the DFT calculation was also carried out to confirm the possible sodium-ion diffusion pathways (Fig. S11). For simplicity, Model 2 (Fig. S11a), in which two [FeO$_6$] octahedra were substituted by two [FeO$_5$] pentahedra according to the maricite type phase structure, was established to approximately simulate locally disordered amorphous structure. As shown in Fig. S11b and S11c, the diffusion barriers of sodium-ion in Model 2 along with Path 1 or Path 2 are much lower than those in Model 1 (pure maricite phase structure). These results indicate that the decreased coordination number of Fe in amorphous phase may create possible sodium-ion diffusion pathways (Fig. 5a).

Conclusion

To study the structure-electrochemical performance relationship, we fabricated a series of NaFePO$_4$ polymorphic composites with different degrees of disorder obtained by tuning the ball-milling parameters. The optimized initial capacity of 115 mAh g^{-1} at 1 C with the capacity retention of 91.3% after 800 cycles was demonstrated, which could be ascribed to the synergistic effect of the active amorphous phase favoring the high sodium-ion storage performance and the inactive ordered maricite phase boosting the structural stability. By using X-ray diffraction and energy-dispersive spectroscopy mapping, high resolution transmission electron microscopy, we revealed the polymorphic composite nature of ordered maricite NaFePO$_4$ crystals embedded into amorphous matrix. Through detailed structural characterizations, we elucidated the atomistic structural origin of the amorphous NaFePO$_4$ being a highly active cathode material for Na-ion batteries, and revealed that the evolution of Fe local surroundings from edge-sharing FeO$_6$ octahedra to FeO$_n$ polyhedra was a key factor for the enhanced electrochemical performances. This work provides a new insight into the atomistic mechanism of the enhanced sodium-ion storage performance for amorphous NaFePO$_4$, and is helpful for developing new battery materials through disorder engineering.

Acknowledgements

References

[1] J.B. Goodenough, K.S. Park, The Li-ion rechargeable battery: a perspective, J. Am. Chem. Soc., 135 (2013) 1167-1176.

[2] C. Delmas, M. Maccario, L. Croguennec, F. Le Cras, F. Weill, Lithium deintercalation in LiFePO4 nanoparticles via a domino-cascade model, Nat. Mater., 7 (2008) 665-671.

[3] L. Guo, Y. Zhang, J. Wang, L. Ma, S. Ma, Y. Zhang, E. Wang, Y. Bi, D. Wang, W.C. McKee, Y.

Xu, J. Chen, Q. Zhang, C. Nan, L. Gu, P.G. Bruce, Z. Peng, Unlocking the energy capabilities of micron-sized LiFePO$_4$, Nat. Commun., 6 (2015) 7898.

[4] A. Paolella, C. Faure, G. Bertoni, S. Marras, A. Guerfi, A. Darwiche, P. Hovington, B. Commarieu, Z. Wang, M. Prato, M. Colombo, S. Monaco, W. Zhu, Z. Feng, A. Vijh, C. George, G.P. Demopoulos, M. Armand, K. Zaghib, Light-assisted delithiation of lithium iron phosphate nanocrystals towards photo-rechargeable lithium ion batteries, Nat. Commun., 8 (2017) 14643.

[5] H. Pan, Y.-S. Hu, L. Chen, Room-temperature stationary sodium-ion batteries for large-scale electric energy storage, Energy Environ. Sci., 6 (2013) 2338-2360.

[6] X. Xiang, K. Zhang, J. Chen, Recent advances and prospects of cathode materials for sodium-ion batteries, Adv. Mater., 27 (2015) 5343-5364.

[7] P.F. Wang, H.R. Yao, X.Y. Liu, Y.X. Yin, J.N. Zhang, Y. Wen, X. Yu, L. Gu, Y.G. Guo, Na$^+$/vacancy disordering promises high-rate Na-ion batteries, Sci. Adv., 4 (2018) eaar6018.

[8] Z. Jian, W. Han, X. Lu, H. Yang, Y.-S. Hu, J. Zhou, Z. Zhou, J. Li, W. Chen, D. Chen, L. Chen, Superior electrochemical performance and storage mechanism of Na$_3$V$_2$(PO$_4$)$_3$ cathode for room-temperature sodium-ion batteries, Adv. Energy Mater., 3 (2013) 156-160.

[9] N. Yabuuchi, K. Kubota, M. Dahbi, S. Komaba, Research development on sodium-ion batteries, Chem. Rev., 114 (2014) 11636-11682.

[10] D. Chao, B. Ouyang, P. Liang, T.T.T. Huong, G. Jia, H. Huang, X. Xia, R.S. Rawat, H.J. Fan, C-plasma of hierarchical graphene survives SnS bundles for ultrastable and high volumetric Na-ion storage, Adv. Mater., 30 (2018) 1804833.

[11] Z. Liu, H. Tan, J. Xin, J. Duan, X. Su, P. Hao, J. Xie, J. Zhan, J. Zhang, J.J. Wang, H. Liu, Metallic intermediate phase inducing morphological transformation in thermal nitridation: Ni$_3$FeN-based three-dimensional hierarchical electrocatalyst for water splitting, ACS Appl Mater Interfaces, 10 (2018) 3699-3706.

[12] W. Tang, X. Song, Y. Du, C. Peng, M. Lin, S. Xi, B. Tian, J. Zheng, Y. Wu, F. Pan, K.P. Loh, High-performance NaFePO$_4$ formed by aqueous ion-exchange and its mechanism for advanced sodium ion batteries, J. Mater. Chem. A, 4 (2016) 4882-4892.

[13] Y. Zhu, Y. Xu, Y. Liu, C. Luo, C. Wang, Comparison of electrochemical performances of

13

olivine $NaFePO_4$ in sodium-ion batteries and olivine $LiFePO_4$ in lithium-ion batteries, Nanoscale, 5 (2013) 780-787.

[14] M. Avdeev, Z. Mohamed, C.D. Ling, J. Lu, M. Tamaru, A. Yamada, P. Barpanda, Magnetic structures of $NaFePO_4$ maricite and triphylite polymorphs for sodium-ion batteries, Inorg. Chem., 52 (2013) 8685-8693.

[15] B.L. Ellis, W.R. Makahnouk, Y. Makimura, K. Toghill, L.F. Nazar, A multifunctional 3.5 V iron-based phosphate cathode for rechargeable batteries, Nat. Mater., 6 (2007) 749-753.

[16] P.P. Prosini, C. Cento, A. Masci, M. Carewska, Sodium extraction from sodium iron phosphate with a Maricite structure, Solid State Ionics, 263 (2014) 1-8.

[17] J. Kim, D.-H. Seo, H. Kim, I. Park, J.-K. Yoo, S.-K. Jung, Y.-U. Park, W.A. Goddard Iii, K. Kang, Unexpected discovery of low-cost maricite $NaFePO_4$ as a high-performance electrode for Na-ion batteries, Energy Environ. Sci., 8 (2015) 540-545.

[18] Y. Liu, N. Zhang, F. Wang, X. Liu, L. Jiao, L.-Z. Fan, Approaching the downsizing limit of maricite $NaFePO_4$ toward high-performance cathode for sodium-ion batteries, Adv. Funct. Mater., 28 (2018) 1801917.

[19] S. Nakata, T. Togashi, T. Honma, T. Komatsu, Cathode properties of sodium iron phosphate glass for sodium ion batteries, J. Non-Cryst. Solids, 450 (2016) 109-115.

[20] R. Kapaev, A. Chekannikov, S. Novikova, S. Yaroslavtsev, T. Kulova, V. Rusakov, A. Skundin, A. Yaroslavtsev, Mechanochemical treatment of maricite-type $NaFePO_4$ for achieving high electrochemical performance, J. Solid State Electrochem., 21 (2017) 2373-2380.

[21] M.M. Rahman, I. Sultana, S. Mateti, J. Liu, N. Sharma, Y. Chen, Maricite $NaFePO_4$/C/graphene: a novel hybrid cathode for sodium-ion batteries, J. Mater. Chem. A, 5 (2017) 16616-16621.

[22] Y. Zhang, P. Wang, T. Zheng, D. Li, G. Li, Y. Yue, Enhancing Li-ion battery anode performances via disorder/order engineering, Nano Energy, 49 (2018) 596-602.

[23] Y. Katayama, S. Hama, T. Yanagihara, M. Hayashi, Manufacturing method for solid electrolyte sheet, U.S. Patent Application No. 12/872,175.

[24] S. Hama, M. Hayashi, Process for producing sulfide-based solid electrolyte, U.S. Patent No.

8,556,197.

[25] B. Delley, From molecules to solids with the DMol3 approach, J. Chem. Phys., 113 (2000) 7756-7764.

[26] J.P. Perdew, K. Burke, M. Ernzerhof, Generalized Gradient Approximation Made Simple, Phys. Rev. Lett., 77 (1996) 3865-3868.

[27] G. Henkelman, B.P. Uberuaga, H. Jónsson, A climbing image nudged elastic band method for finding saddle points and minimum energy paths, J. Chem. Phys., 113 (2000) 9901-9904.

[28] K. Zaghib, J. Trottier, P. Hovington, F. Brochu, A. Guerfi, A. Mauger, C.M. Julien, Characterization of Na-based phosphate as electrode materials for electrochemical cells, J. Power Sources, 196 (2011) 9612-9617.

[29] R. Rajagopalan, B. Chen, Z. Zhang, X.L. Wu, Y. Du, Y. Huang, B. Li, Y. Zong, J. Wang, G.H. Nam, M. Sindoro, S.X. Dou, H.K. Liu, H. Zhang, Improved reversibility of Fe^{3+}/Fe^{4+} redox couple in sodium super ion conductor type $Na_3Fe_2(PO_4)_3$ for sodium-ion batteries, Adv. Mater., 29 (2017) 1605694.

[30] X. Deng, W. Shi, J. Sunarso, M. Liu, Z. Shao, A green route to a Na_2FePO_4F-based cathode for sodium ion batteries of high rate and long cycling life, ACS Appl Mater Interfaces, 9 (2017) 16280-16287.

[31] X.H. Wu, G.M. Zhong, Y. Yang, Sol-gel synthesis of $Na_4Fe_3(PO_4)_2(P_2O_7)/C$ nanocomposite for sodium ion batteries and new insights into microstructural evolution during sodium extraction, J. Power Sources, 327 (2016) 666-674.

[32] B. Shen, M. Xu, Y. Niu, J. Han, S. Lu, J. Jiang, Y. Li, C. Dai, L. Hu, C. Li, Sodium-rich ferric pyrophosphate cathode for stationary room-temperature sodium-ion batteries, ACS Appl Mater Interfaces, 10 (2018) 502-508.

[33] M. Chen, L. Chen, Z. Hu, Q. Liu, B. Zhang, Y. Hu, Q. Gu, J.L. Wang, L.Z. Wang, X. Guo, S.L. Chou, S.X. Dou, Carbon-coated $Na_{3.32}Fe_{2.34}(P_2O_7)_2$ cathode material for high-rate and long-life sodium-ion batteries, Adv. Mater., 29 (2017) 1605535.

[34] J.C. Zheng, B.Y. Yang, X.W. Wang, B. Zhang, H. Tong, W.J. Yu, J.F. Zhang, Comparative investigation of $Na_2FeP_2O_7$ sodium insertion material synthesized by using different sodium sources,

ACS Sustainable Chem. Eng., 6 (2018) 4966-4972.

[35] D.R. McKenzie, D. Muller, B.A. Pailthorpe, Compressive-stress-induced formation of thin-film tetrahedral amorphous carbon, Phys. Rev. Lett., 67 (1991) 773-776.

[36] Sturman B D, Mandarino J A, C.M. I., Maricite, a sodium iron phosphate, from the Big Fish River area, Yukon Territory, Canada, Can. Mineral., 15 (1977) 396-398.

[37] Le Page Y, D. G., The crystal structure of the new mineral maricite, $NaFePO_4$, Can. Mineral., 15 (1977) 518-521.

[38] G. Wu, K.C. Chan, L. Zhu, L. Sun, J. Lu, Dual-phase nanostructuring as a route to high-strength magnesium alloys, Nature, 545 (2017) 80-83.

[39] D. Wang, X. Wu, Z. Wang, L. Chen, Cracking causing cyclic instability of $LiFePO_4$ cathode material, J. Power Sources, 140 (2005) 125-128.

[40] S. Watanabe, M. Kinoshita, T. Hosokawa, K. Morigaki, K. Nakura, Capacity fade of $LiAl_yNi_{1-x-y}Co_xO_2$ cathode for lithium-ion batteries during accelerated calendar and cycle life tests (surface analysis of $LiAl_yNi_{1-x-y}Co_xO_2$ cathode after cycle tests in restricted depth of discharge ranges), J. Power Sources, 258 (2014) 210-217.

[41] F. Xiong, S. Tan, Q. Wei, G. Zhang, J. Sheng, Q. An, L. Mai, Three-dimensional graphene frameworks wrapped $Li_3V_2(PO_4)_3$ with reversible topotactic sodium-ion storage, Nano Energy, 32 (2017) 347-352.

[42] H. Tan, Z. Liu, D. Chao, P. Hao, D. Jia, Y. Sang, H. Liu, H.J. Fan, Partial nitridation-induced electrochemistry enhancement of ternary oxide nanosheets for fiber energy storage device, Adv. Energy Mater., 8 (2018) 1800685.

[43] T. Jawhari, A. Roid, J. Casado, Raman spectroscopic characterization of some commercially available carbon black materials, Carbon, 33 (1995) 1561-1565.

[44] S.-M. Oh, S.-T. Myung, J. Hassoun, B. Scrosati, Y.-K. Sun, Reversible $NaFePO_4$ electrode for sodium secondary batteries, Electrochem. Commun., 22 (2012) 149-152.

[45] P. Moreau, D. Guyomard, J. Gaubicher, F. Boucher, Structure and stability of sodium intercalated phases in olivine $FePO_4$, Chem. Mater., 22 (2010) 4126-4128.

[46] A. Angell, Thermodynamics: liquid landscape, Nature, 393 (1998) 521-524.

[47] F.M.F. de Groot, M. Grioni, J.C. Fuggle, J. Ghijsen, G.A. Sawatzky, H. Petersen, Oxygen 1sx-ray-absorption edges of transition-metal oxides, Physical Review B, 40 (1989) 5715-5723.

[48] J. Purans, A. Kuzmin, P. Parent, C. Laffon, X-ray absorption study of the electronic structure of tungsten and molybdenum oxides on the O K-edge, Electrochim. Acta, 46 (2001) 1973-1976.

[49] R.S. Cole, R. Frech, Spectroscopic characterization of pure and cation-stabilized sodium phosphate, J. Chem. Phys., 112 (2000) 4251-4261.

[50] L. Ma, R.K. Brow, A. Choudhury, Structural study of Na_2O-FeO-Fe_2O_3-P_2O_5 glasses by Raman and Mossbauer spectroscopy, J. Non-Cryst. Solids, 402 (2014) 64-73.

[51] D.J.M. Burkhard, Iron-bearing silicate glasses at ambient conditions, J. Non-Cryst. Solids, 275 (2000) 175-188.

[52] S.S. Shinde, S.S. Meena, S.M. Yusuf, K. Y. Rajpure, Mossbauer, Raman, and magnetoresistance study of aluminum-based iron oxide thin films, J. Phys. Chem. C 115 (2011) 3731–3736.
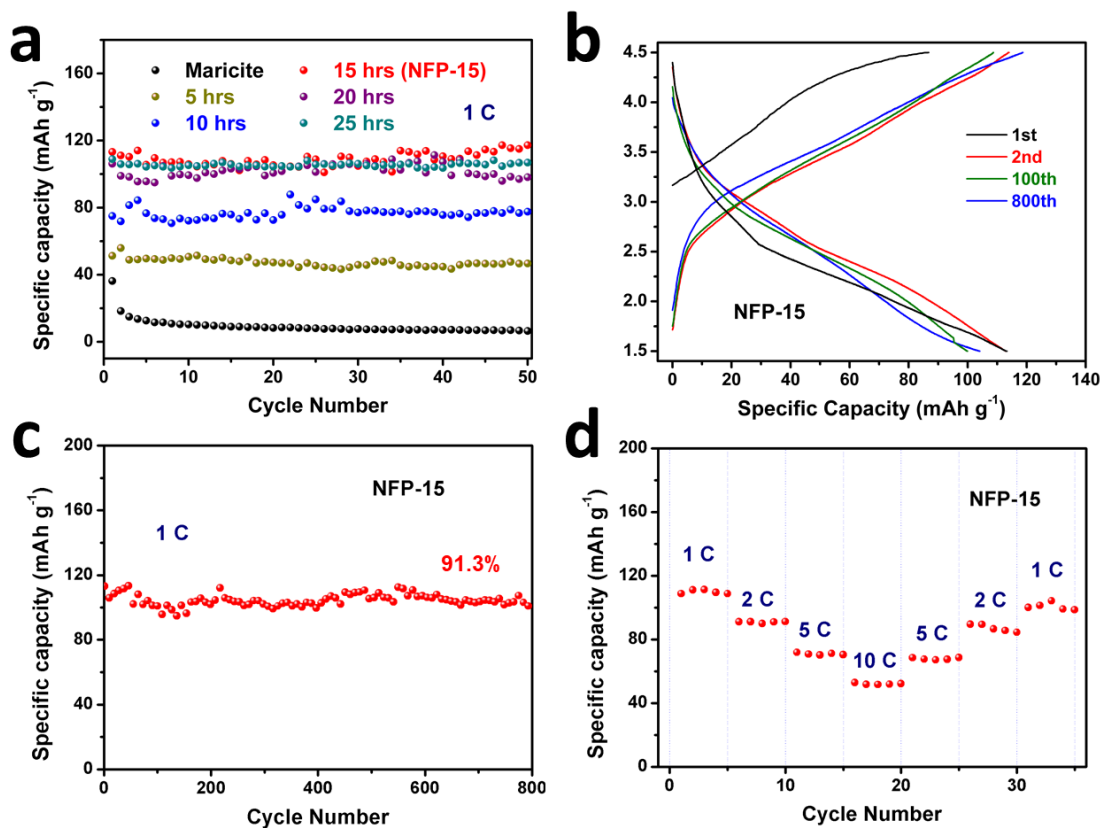
Fig. 1 Sodium-ion storage performance. (a) Cycling stability at 1 C (1 C = 155 mA g^{-1}) of the polymorphic composites obtained by milling at 600 rpm for 5, 10, 15, 20, and 25 hours, together with the as-prepared maricite NaFePO$_4$; (b) The charge/discharge curves at 1C of the polymorphic composites obtained by milling at 600 rpm for 15 hours (NFP-15); (c) The long-term cycling stability up to 800 cycles at 1 C of NFP-15. (d) The rate performance of NFP-15; The voltage window is within the range of 1.5 and 4.5 V, sodium pellet as the anode, and NaPF$_6$ with 1 mol L^{-1} dissolved in an equal volume ratio EC-PC solution as the electrolyte.
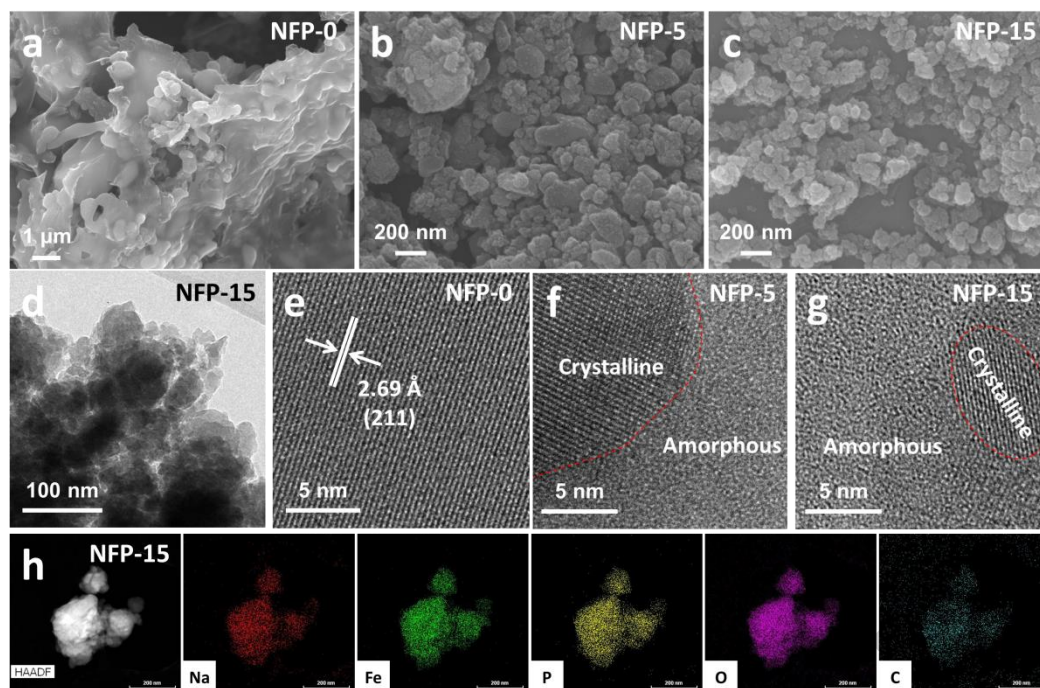
Fig. 2 Structure and morphology of polymorphic composites. (a-c) FESEM images of the as-prepared maricite NaFePO$_4$ (a), polymorphic composites obtained by milling at 600 rpm for 5 hrs (b) and 15 hrs (NFP-15) (c). (d) The TEM image of NFP-15; (e-g) HRTEM images of the as-prepared maricite NaFePO$_4$(e), polymorphic composites obtained by milling at 800 rpm for 5 hrs (f) and 15 hrs (g); (h) The HAADF image together with EDS elemental mappings of Na, Fe, P, O, C for NFP-15.
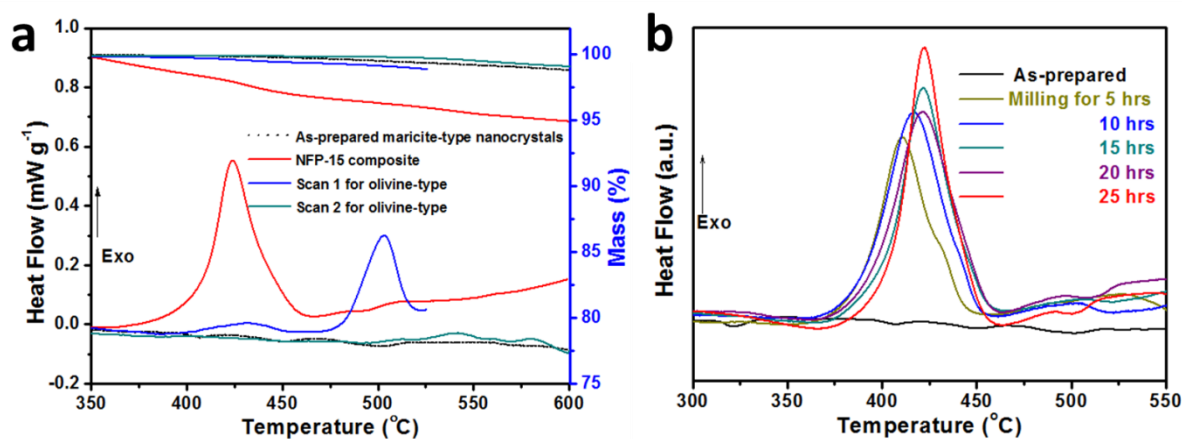
Figure 3 Phase transitions of NaFePO$_4$ on heating. (a) Calorimetric plots of polymorphic composites through milling for 5, 10, 15 (NFP-15), 20, 25 hrs together with the as-prepared maricite-type NaFePO$_4$. (b) Thermo-gravimetric analysis and calorimetric plots, showing the exothermic recrystallization peaked at 425 ℃ of the NFP-15 composite, as well as the apparent irreversible phase transition peaked at 500 ℃ from olivine-type to maricite-type NaFePO$_4$.
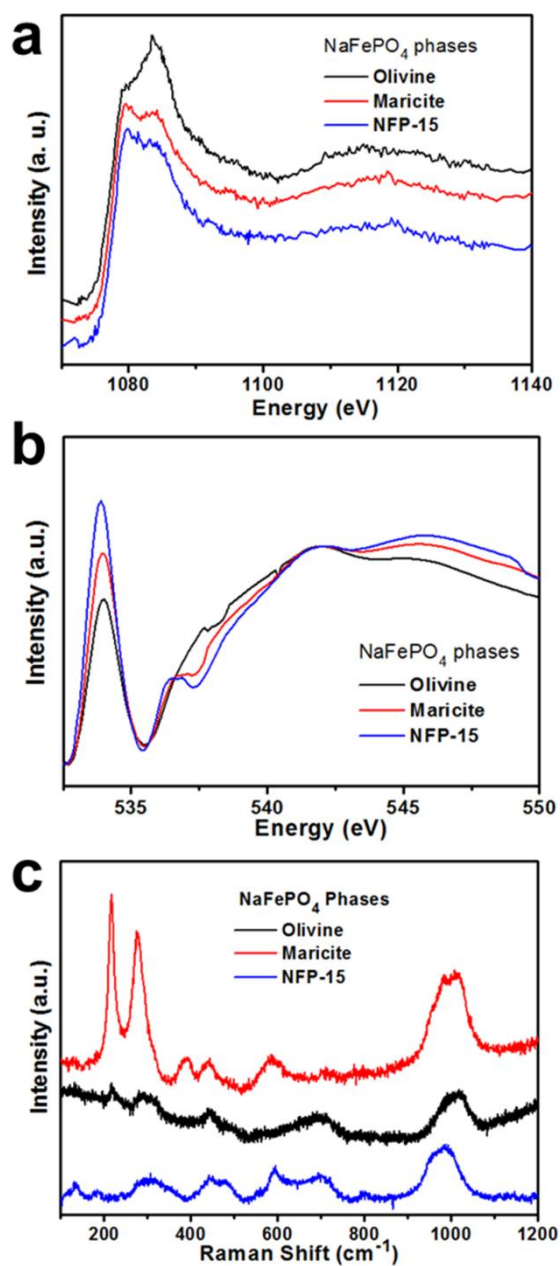
Fig. 4 Structural differences of NaFePO₄ phases. X-ray absorption near edge structure spectra of

(a) Na K-edge, (b) O K-edge for olivine-type, maricite-type and polymorphic composites obtained

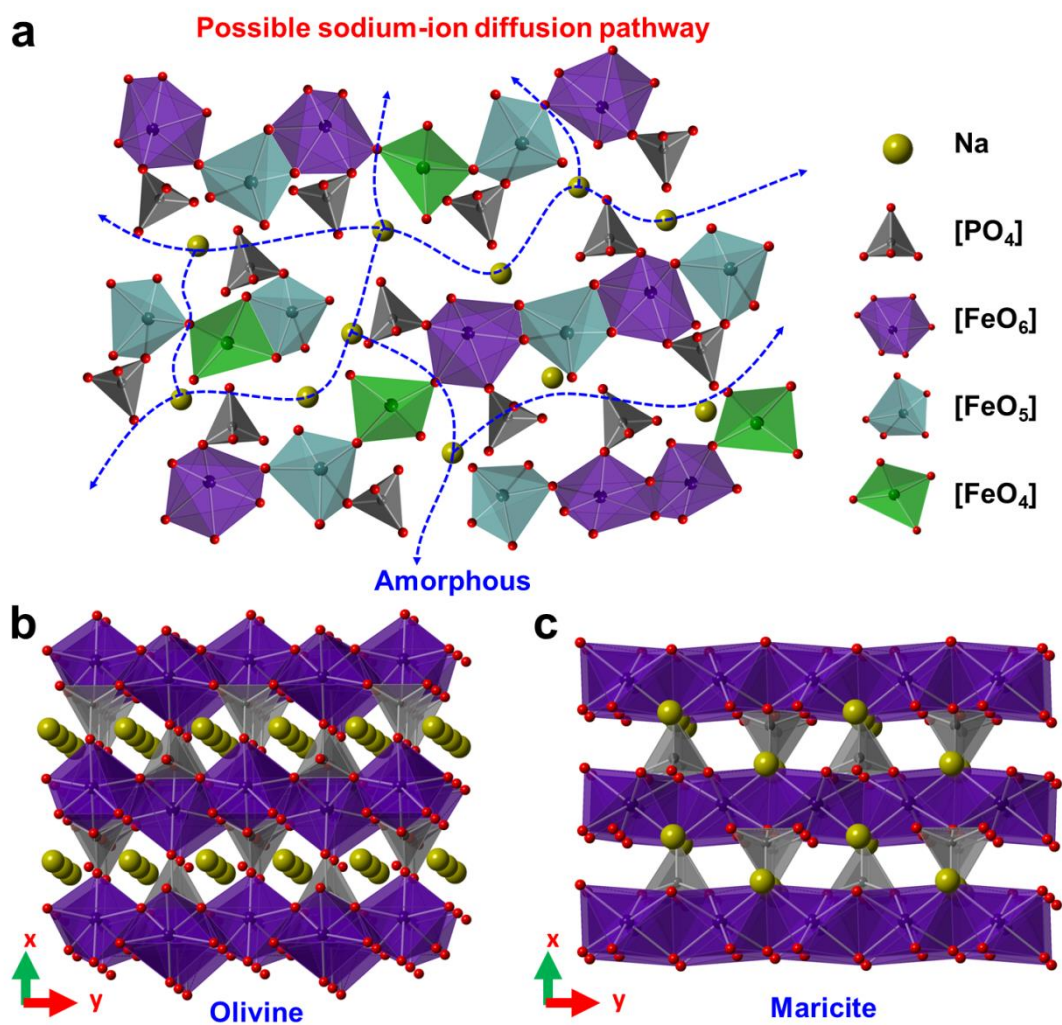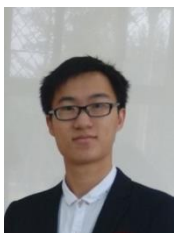by milling for 15 hrs (NFP-15), together with their Raman spectra (c).

Fig. 5 Schematic illustrations for Na diffusive mechanism. (a) Possible sodium-ion diffusive pathways and atomistic structure for amorphous $NaFePO_4$. Structural sketching diagrams of (b) olivine-type $NaFePO_4$ and (c) maricite-type $NaFePO_4$.

Fangyu Xiong received his B.S. degree in Material Physics from Wuhan University of Technology in 2016. He is currently working toward the Ph.D. degree and his current research interests focuses on electrode materials for emerging energy storage devices.
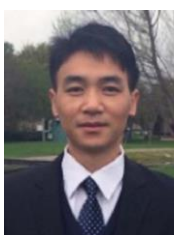
Qinyou An is Associate Professor of Materials Science and Engineering at Wuhan University of Technology (WUT). He received his Ph.D. degree from WUT in 2014. He carried out his postdoctoral research in the laboratory of Prof. Yan Yao at the University of Houston in 2014-2015. Currently, his research interest includes energy storage materials and devices.

Lixue Xia is currently a Ph.D. candidate in School of materials science and engineering at Wuhan University of technology. His research areas are nanomaterial simulation and design of new efficient electrocatalyst guided by the First principles calculation.

Yan Zhao is Chair Professor of Materials Science at Wuhan University of Technology. He received a Ph.D. degree in Chemistry from the University of Minnesota in 2005. His research areas are computational materials science, density functional theory, nano-materials simulation, computational catalysis, theoretical organic chemistry, and 3D printing. He is in the "Highly Cited Researcher" list four times in a row in 2014-2017. He is the author of over 70 scientific papers and 25 patent applications worldwide, and he is the coauthor of four computational chemistry software programs including MLGAUSS, MULTILEVL, Q-Chem, and NWChem.

Liqiang Mai is Chair Professor of Materials Science and Engineering at Wuhan University of Technology (WUT). He received his Ph.D. from WUT in 2004. He carried out his postdoctoral research in the laboratory of Prof. Zhonglin Wang at Georgia Institute of Technology in 2006–2007 and worked as advanced research scholar in the laboratory of Prof. Charles M. Lieber at Harvard University in 2008–2011. His current research interests focus on nanowire materials and devices for energy storage. He received the National Natural Science Fund for Distinguished Young Scholars, the First Prize for Hubei Natural Science Award and so forth.

Haizheng Tao is Chair Professor of State Key Laboratory of Silicate Materials for Architectures at Wuhan University of Technology (WUT). He received his Ph.D. from WUT in 2004. He is the author of over 150 scientific papers and 31 granted patent. He is the vice chair of Special Glass Branch of the Chinese Ceramic Society. His current research interests focus on optical materials, energy storage materials, glasses and amorphous materials.

Yuanzheng Yue is Professor of Chemistry at Aalborg University (AAU), Denmark, and a distinguished visiting professor at Wuhan University of Technology, China. He received his Ph.D. degree from Technische Universität Berlin, Germany, in 1995. He is the founding head of Center for Amorphous Materials Science at AAU, Denmark. He is a council member of the International Commission on Glass (ICG). He is the founding chair of the ICG Technical Committee for Glass Fibers. His research focuses on glasses, glass fibres, insulation materials, and amorphous materials for energy storage devices.

Highlights

- The atomistic origin of the enhanced Na-storage performance of amorphous $NaFePO_4$ was uncovered.

- We succeeded in tuning the degree of disorder in $NaFePO_4$ cathode material by a mechanochemical route.

- The excellent cycling stability (capacity retention of 91.3% after 800 cycles) was attained.